Sustainable Energy Technologies and Assessments 48 (2021) 101634

Contents lists available at ScienceDirect

Sustainable Energy Technologies and Assessments

journal homepage: www.elsevier.com/locate/seta

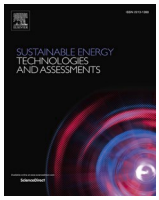

Original article

Comparative evaluation of two photovoltaic multi-pump parallel system configurations for optimal distribution of the generated power

María Gasque [a], Pablo González-Altozano [b,*], Rosa Penélope Gutiérrez-Colomer [b], Eugenio García-Marí [b]

[a] Dept. Física Aplicada, Universitat Politècnica de València, Camino de Vera s/n, 46022 Valencia, Spain
[b] Dept. Ingeniería Rural y Agroalimentaria, Universitat Politècnica de València, Camino de Vera s/n, 46022 Valencia, Spain

ARTICLE INFO

Keywords:
Pumping system
Energy optimisation
Parallel pumps
System performance
Simulation

ABSTRACT

The suitability of a strategy for distributing the power generated by a photovoltaic pumping system equipped with two equal pumps working in parallel is proven. This strategy aims to improve energy management and consists of feeding a single pump with all the power generated until it exceeds a threshold value from which the power distribution must be at 50% between the two pumps. This pumping method was compared with the operation mode usually applied in parallel PV pumping facilities (50% of the power always assigned to each pump). A system equipped with two 0.75 kW pumps was employed. The assessment of the facility's performance under the two alternative working conditions and several pumping heads was conducted using simulation techniques. Both the pumped annual volume and the annual efficiency of the motor-pump group increased when the strategy was applied compared to operation with power distribution at 50%. This increase was greater the higher the head (6.21% at H = 18 m vs. 57.60% at H = 48 m for pumped annual volume and 6.42% at H = 18 m vs. 57.51% at H = 48 m for annual efficiency). The halving of the irradiance threshold and the improved efficiency (36.4% vs. 34.8%) may explain this increase.

Introduction

The use of renewable energies is constantly increasing, providing an environmentally friendly alternative to conventional energy sources. They contribute to a large extent to sustainable development as they reduce the reliance on fossil fuels and play an important role in greenhouse gas emission decrease. In this context, it is also worth noting the significant growth of photovoltaic (PV) and wind technologies [1–3]. Among solar photovoltaic uses, water pumping is one of the most promising applications, with many economic and environmental benefits compared to traditional options and enabling the development of low carbon irrigated agriculture [4].

A PV pumping facility converts solar irradiance into hydraulic energy. The three main components in a PV pumping system are the PV generator, the power conditioning unit, and the motor-pump group. The PV generator absorbs the radiant solar energy and transforms it into electricity, which will be used to feed the pump. The power conditioning unit in alternating current (AC) systems is a variable speed drive (VSD), which converts the direct current (DC) output of the PV field into AC to feed the motor-pump group with the appropriate current/voltage/frequency. The VSD also adjusts the operating point of the PV generator to its maximum power conditions or to the pump power demand. Finally, the motor-pump group transforms electricity into hydraulic power. In medium and large size PV pumping systems, AC centrifugal pumps are often used.

As PV pumping facilities became one of the most affordable solutions, its use has become widespread in remote rural areas of developing countries to supply drinking water for human or livestock [5,6], for irrigation in agriculture [7,8], or in some cases to address issues with grid supply [9]. Solar pumping facilities are also widely used in developed countries for the irrigation of many crops, mainly in areas with high solar irradiance levels [10–12]. Consequently, there has been a continuous development of more powerful and efficient solar-powered pumping equipment [4,13]. The great variability of incident solar radiation and, thus, available power, implies that the facilities must be carefully sized, paying attention to their design and optimal use, to provide adequate energy management and minimize the system cost [7,14,15].

To improve system energy efficiency and reduce both the effect of

* Corresponding author.
E-mail address: pgaltozano@agf.upv.es (P. González-Altozano).

https://doi.org/10.1016/j.seta.2021.101634
Received 11 April 2021; Received in revised form 18 September 2021; Accepted 23 September 2021
Available online 6 October 2021

Nomenclature

H (m)	Pumping head
P (kW)	Electric power supplied to the motor-pump group
P_e (kW)	Power value from which the two pumps operate in parallel with a 50% power distribution.
P_{max} (kW)	Maximum power to motor-pump
Q (L/s)	Flow rate
q(P) (L/s)	Flow rate propelled by one pump
Q(P) (L/s)	Flow rate propelled by the two pumps operating in parallel.

Greek symbol

η_{mp}	Efficiency of motor-pump group

Acronyms

AC	Alternating current
DC	Direct current
FC	Frequency converter
PV	Photovoltaic
SI	Solar irradiation (kWh/m^2)
STC	Standard test conditions
TMY	Typical meteorological year
VSD	Variable speed drive

irradiance fluctuations and the power threshold to start pumping, different alternatives and technical solutions to pump a certain water volume at the required head may be adopted. Many studies have been published giving diverse solutions to this topic and some of them are worth mentioning. Thus, a pump selection method based on considering the efficiency in the whole range of operating frequencies was proposed in [16]. This way, power threshold to start pumping was reduced, achieving longer periods of pumping. In [17], a reconfigurable PV Array based water pumping scheme was proposed that allowed the pump to operate under low irradiance conditions and produce greater output power. Some solutions to solve the problems associated to power intermittency and to match photovoltaic production with irrigation demand were proposed in [18], while in [19] a scheme which resulted in more pumped water under variable pumping heads was presented. It is also worth noting the review by Poompavai and Kowsalya [20] that addressed control and energy management strategies in PV solar water pumping systems, and the approach in [21] based on the simultaneous operation of a variable number of irrigation sectors according to the available energy that provides the optimal performance of the system.

Currently, there are a considerable number of photovoltaic pumping facilities with two or more pumps connected in parallel. This configuration is an alternative that is well adapted to the variable demand for water flow, avoiding as much as possible the effect of fluctuations in climate and irradiance. The use of several pumps working in parallel may also improve the efficiency of the facility and increase the daily operating time [22]. Proper management of the available photovoltaic power leads to both a reduction in the irradiance threshold required for pumping (pumping starts earlier and ends later), and greater efficiency during operating hours with less insolation, since with low powers the system can work with fewer pumps and the different pumps can be connected or disconnected depending on the available power. On the other hand, in PV facilities equipped with multi-pump parallel groups, it is possible to install an independent PV generator for each pump. Another option is to use a single PV generator to supply the entire facility and establish either a strategy of equal distribution of the generated power among the different pumps or a more efficient distribution strategy that allows for optimising the flow rate pumped by the facility at any time.

Further studies related to this type of facilities are necessary to improve their management and determine the working sequence of the pumps that optimises the distribution of photovoltaic power and maximises the use of energy. In order to meet this need, Gasque et al. [23] proposed and mathematically justified a method for distributing the power generated in a photovoltaic parallel pumping system equipped with two equal pumps and a single generator. An optimal division for the available power was suggested with the intention of maximizing the pumped flow rate and allowing the pumps to pump at lower irradiance levels.

The main objective of the present paper is to verify the suitability of that methodology. To that end, pumping by applying the strategy of dividing the generated power was compared with pumping with the generated power distribution at 50% between the two motor-pump groups at all times, which is the usual operation mode in parallel PV pumping facilities. The study and comparative analysis of the facility's performance under the two working conditions, and pumping at several heads, was carried out using simulation techniques.

It should be noted that the option of operating with power distribution at 50% between the two pumps (hereafter referred to as Distribution at 50%) is equivalent to considering the facility equipped with two equal PV generators. With this configuration, each generator transfers the electrical power generated to its corresponding frequency converter-motor pump group. Implementing a power distribution strategy between the two pumps (hereafter referred to as Strategy) is equivalent to considering a single PV generator for both pumps. In this case, the power coming from the PV generator is applied to the pumps through their respective frequency converter (FC), which can modulate the power supplied to each pump through the frequency/output voltage control.

To accomplish the main objective, mathematical modelling was carried out for both the components of the facility and the energy losses in the photovoltaic generator. Afterwards, simulations of the annual operation of the PV system were performed in LabVIEW using the results obtained from the experimental characterisation tests of the motor-pump group and employing the climatic values of a typical meteorological year (TMY) developed for Valencia, Spain.

The comparison of the two working modes was made from the estimation of both the pumped volume and the efficiency of the pumping group at the different pumping heads.

This paper offers an appropriate solution to supply water needs for irrigation and human consumption in developing countries as it is suggested a novel design and management of photovoltaic pumping facilities, easy to implement and set up, that optimises water pumping efficiency.

Research background and power distribution strategy

In this section, the key issues of the strategy for distributing the power generated between two equal parallel pumps are reviewed.

Experimental characterisation of the motor-pump group

The behaviour of a standalone PV pumping facility with two 0.75 kW centrifugal pumping groups working in parallel on the same hydraulic network, was investigated. The experimental characterisation of the pumping group to determine the flow rate-head (Q-H), flow rate-electric power (Q-P), and flow rate-motor pump efficiency (Q-η_{mp}) curves at different working frequencies was performed. The frequencies tested were 50, 45, 40, 35 and 30 Hz and the pumping heads considered were 18, 24, 30, 36, 42, and 48 m. The values of Q and P obtained in the experimental trials at each head H were adjusted by regression using a fourth-degree polynomial function, q(P).

The experimental tests were carried out in the hydraulic laboratory at the Universitat Politècnica de València. The experimental setup is described in more detail in [23].

Distribution of the generated power between the two pumps

The results concerning the flow rate pumped at each working condition and the distribution ratio of the generated power showed some differences between higher and lower heads. However, in both cases a power value was found, referred to as P_e, above which the available power should be distributed at 50% between the two pumps. By contrast, if the power is lower than this threshold value, all the available power must be assigned to only one of the pumps.

The determination of P_e was established analytically from the curves representing the flow rate-power relationship of a single pump (q(P)) and the two pumps (Q(P)) with the distribution of the generated power at 50%. The analysis derived from this graphic representation led to considering two cases, named (a) and (b) (Fig. 1). In case (a), the curves q(P) and Q(P) intersect at a value of $P < P_{max}$ and it corresponded with lower pumping heads. In case (b), the curves q(P) and Q(P) do not intersect and it corresponded with higher heads. It was proven that the optimal distribution strategy of the available power depends on whether $P_e > P_{max}$ (higher heads) or $P_e < P_{max}$ (lower heads).

In practice, it is possible to determine whether pumping at a certain head corresponds to case (a) or (b) by a simple pumping test. Since $Q(P_{max}) = 2q(P_{max}/2)$, it would be sufficient to carry out a pumping test with a single pump and to check whether $q(P_{max})$ is lower (case a) or higher (case b) than $2q(P_{max}/2)$.

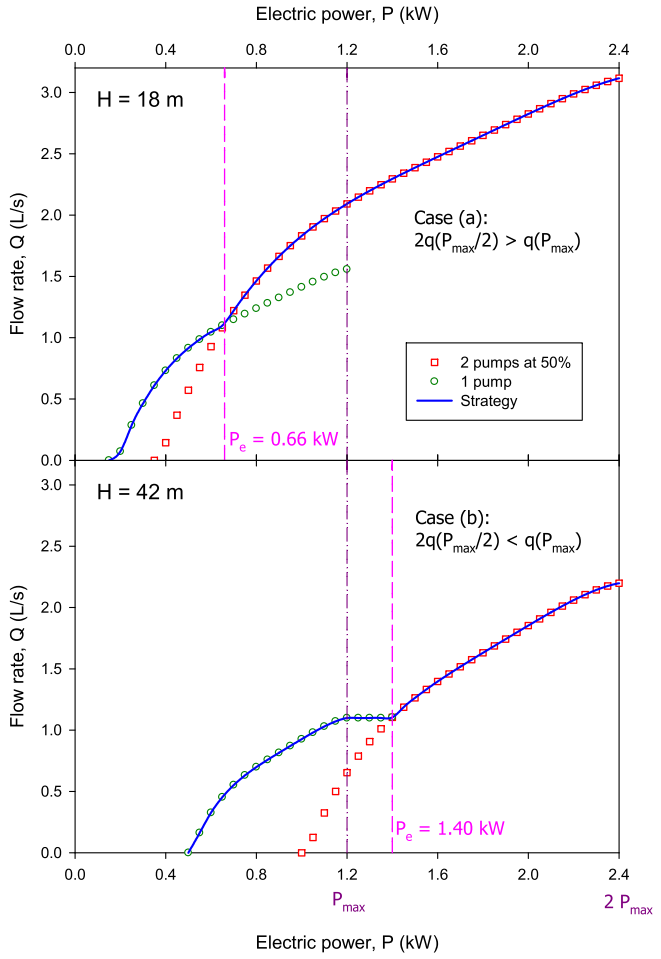

Fig. 1. Flow rate-power curves of a single 0.75 kW pump, two 0.75 kW centrifugal pumps in parallel with power distribution at 50%, and power distribution strategy. Pumping at H = 18 m (case (a), $P_e < P_{max}$), and at H = 42 m (case (b), $P_e > P_{max}$).

Materials and methods

Mathematical model of the components of the facility

Photovoltaic generator

PV modules and configuration of the PV generator. For the configuration of the photovoltaic generator, polycrystalline silicon PV modules (A-127P model, manufactured by Atersa) with 36 cells connected in series were selected.

The characteristics of the PV module [24] are shown in Table 1.

The nominal power of each pumping group is the power on the pump shaft, in this case, 0.75 kW. The electrical power supplied must be somewhat higher to compensate for the efficiency of the electric motor. According to the manufacturer's catalogue [25], the efficiency of the electric motor under nominal conditions is 70%. The maximum power supply must, therefore, be 1.07 kW.

The peak power of the PV generator is increased 10–20% by taking into account the efficiency of the frequency converter (≈0.95), the losses in the PV generator (e.g. increase in cell temperature, losses due to inefficiencies derived from the series–parallel connection) compared to its operation under standard test conditions (STC), and the losses in the wiring. Thus, the maximum power of the PV generator for the two 0.75 kW pump groups, is approximately $1.07 \times 1.2 \times 2 = 2.56$ kWp.

The PV generator was then configured with 20 polycrystalline silicon solar modules of 127 Wp connected in series, able to provide 2540 kWp of total power. In this manner, the voltage at the maximum power point (MPP) of the generator in working conditions (cell temperature, $T_c = 50\ ^\circ C$) was around 303 V, within the reasonable limits of the input range of DC to the FC.

In any case, if at any moment in the year more electrical power could be generated than pumping groups allow, the MPPT (maximum power point tracking) system of the frequency converter automatically shifts the operating point of the PV generator to limit the electrical power generated to the maximum allowed value.

PV generator mathematical model. A single-diode model with five parameters was used to simulate the PV module performance. In this circuit model, often used in the literature (Fig. 2), the current–voltage (I-V) relationship is given by an implicit, non-linear equation:

$$I = I_L - I_D - I_P = I_L - I_0\left[\exp\left(\frac{V + IR_s}{mV_t}\right) - 1\right] - \frac{V + IR_s}{R_{sh}} \quad (1)$$

where:

I(A) is the cell current
V(V) is the cell voltage
I_L (A) is the light-generated current
I_D (A) is the diode current

Table 1
Specifications of the PV module [24].

Electrical characteristics (STC: G = 1 kW/m^2, AM 1,5, T_{cel} = 25 °C)	
Nominal Power (±5%)	127 W
Current at Maximum Power Point (I_{mp})	7.28 A
Voltage at Maximum Power Point (V_{mp})	17.48 V
Short-Circuit Current (I_{sc})	7.95 A
Open-Circuit Voltage (V_{oc})	22.05 V
Thermal Parameters	
Temperature Coefficient of I_{sc} (α_I)	2.30 mA/°C
Temperature Coefficient of V_{oc} (α_V)	−76.32 mV/°C
Nominal Operating Cell Temperature (NOCT)	47 ± 2 °C
Physical Characteristics	
Dimensions (mm)	1476x659x35
Weight (kg)	12.80

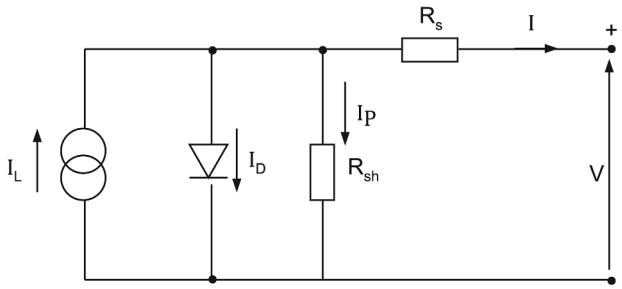

Fig. 2. Single-diode solar cell model electrical equivalent circuit.

I_P (A) is the shunt resistant current
I_0 (A) is the diode reverse saturation current
$m = N_s{\cdot}n$ (where N_s is the number of solar cells connected in series and n is the diode ideality factor, which indicates solar cell characteristic deviation from ideal behaviour)
R_s (Ω) is the series resistance of the cells
R_{sh} (Ω) is the shunt resistance

The terms I_L, I_0, m, R_s and R_{sh} are five parameters that depend on the cell temperature and the incident solar radiation.

V_t (V) is the thermal voltage, which depends on the cell temperature, T_c (K), and is defined by:

$$V_t = \frac{k_B T_c}{q} \tag{2}$$

where k_B is Boltzmann's constant ($1{,}38065{\cdot}10^{-23}$ J/K) and q is the electron charge ($1{,}602176{\cdot}10^{-19}$ C).

The analytical method reported by Phang et al. [26] was employed to estimate the five parameters of the model equation under particular operating conditions (solar irradiance and cell temperature). This method makes some approximations or simplifying assumptions that allow obtaining the model parameters from the electrical characteristics of the photovoltaic module, supplied by the manufacturer in STC (short-circuit current I_{sc}, open-circuit voltage V_{oc}, and current and voltage at the MPP I_{mp}, V_{mp}). The determination of R_{so} and R_{sho}, which represent the reciprocal of the slope at the open-circuit point and the reciprocal of the slope at the short-circuit point, respectively, is also required.

$$R_{so} = -\left(\frac{\partial V}{\partial I}\right)_{V=V_{oc}} \tag{3}$$

$$R_{sho} = -\left(\frac{\partial V}{\partial I}\right)_{I=I_{sc}} \tag{4}$$

The following equations were used to calculate the five parameters required:

$$R_{sh} = R_{sho} \tag{5}$$

$$m = \frac{V_{mp} + I_{mp}{\bullet}R_{so} - V_{oc}}{V_t\left[\ln\left(I_{sc} - \frac{V_{mp}}{R_{sh}} - I_{mp}\right) - \ln\left(I_{sc} - \frac{V_{oc}}{R_{sh}}\right) + \frac{I_{mp}}{I_{sc} - \frac{V_{oc}}{R_{sh}}}\right]} \tag{6}$$

$$I_0 = \left(I_{sc} - \frac{V_{oc}}{R_{sh}}\right)\exp\left(-\frac{V_{oc}}{mV_t}\right) \tag{7}$$

$$R_s = R_{so} - \left[\frac{mV_t}{I_0}\exp\left(-\frac{V_{oc}}{mV_t}\right)\right] \tag{8}$$

$$I_L = I_{sc}\left(1 + \frac{R_s}{R_{sh}}\right) + I_0\left[\exp\left(-\frac{I_{sc}R_s}{mV_t}\right) - 1\right] \tag{9}$$

Once calculated, the five parameters were applied in Eq. (1), thus, obtaining the I-V characteristics in STC. The good accuracy and the validity of this method have been proven by several authors [27–29].

Modelling a PV generator must make it possible to predict the generated electric power under any operating conditions. To achieve this, the current–voltage (I-V) characteristics of the PV module must be adapted to different conditions defined by the ambient temperature (T_a) and the solar irradiance (G). With this aim, the geometric translation model presented in [30] was applied. This method consists of translating the obtained I-V curve to the desired operating conditions. It is based on the prior obtaining of I_{sc} and V_{oc} values under the new operating conditions using the coefficients of variation of these parameters with temperature (commonly provided by manufacturers of solar modules).

Previously, the cell temperature under operating conditions, T_c (°C), which is determined using the thermal model, was estimated by:

$$T_c = T_a + \frac{NOCT - 20}{800}G \tag{10}$$

where NOCT (°C) is the nominal operating cell temperature, T_a (°C) is the ambient air temperature, and G (W/m^2) is solar irradiance.

To calculate the short-circuit current (I_{sc}) and the open-circuit voltage (V_{oc}), the following expressions were used:

$$I_{sc} = I_{sc}^{*}\frac{G}{G^{*}} + \alpha_I(T_c - T_c^{*}) \tag{11}$$

$$V_{oc} = V_{oc}^{*} + mV_t\ln\frac{G}{G^{*}} + \alpha_V(T_c - T_c^{*}) \tag{12}$$

where the superscript * indicates that the value is referred to the STC and α_I and α_V are the temperature coefficients of I_{sc} and V_{oc}, respectively, which are provided by the manufacturer (Table 1).

Finally, the translation of the (I*-V*) curve from STC to working conditions was performed using the expressions:

$$I = I^{*} + \left(I_{sc} - I_{sc}^{*}\right) \tag{13}$$

$$V = V^{*} + \left(V_{oc} - V_{oc}^{*}\right) \tag{14}$$

This procedure has been experimentally applied and validated giving accurate results when comparing simulated vs. measured I-V curves [30,31].

Once the points I and V of the curve were obtained in the new operating conditions, the values of the intensity and the voltage at the point of maximum power, I_{mp}, V_{mp}, and the electrical power generated by the module and the PV generator were estimated.

A diagram of the mathematical model of the PV module and its application to determine the power generated at any working condition is included in Fig. 3.

Energy loss mechanisms. The energy losses in the PV generator considered were the following:

- Losses due to the angle of incidence of solar radiation and dust over the PV module's surface. The model proposed by Martin and Ruiz [32] was used to determine the effect of the angle of incidence of solar radiation on the reflectance and transmittance of the glass that covers the PV modules. An average degree of dirt was assumed.
- Losses due to the increase in cell temperature above 25 °C.
- Connection losses: losses in wiring by Joule effect of 6% of the maximum power generated have been assumed.

Frequency converter

An Altivar 61 (HU30M3 model), was used as a variable speed drive to feed the motor-pump group, allowing modifying the electric power and the flow rate pumped.

As stated in [33], the FC can be considered as an inverter that can modulate the output signal to the desired frequency and amplitude. The

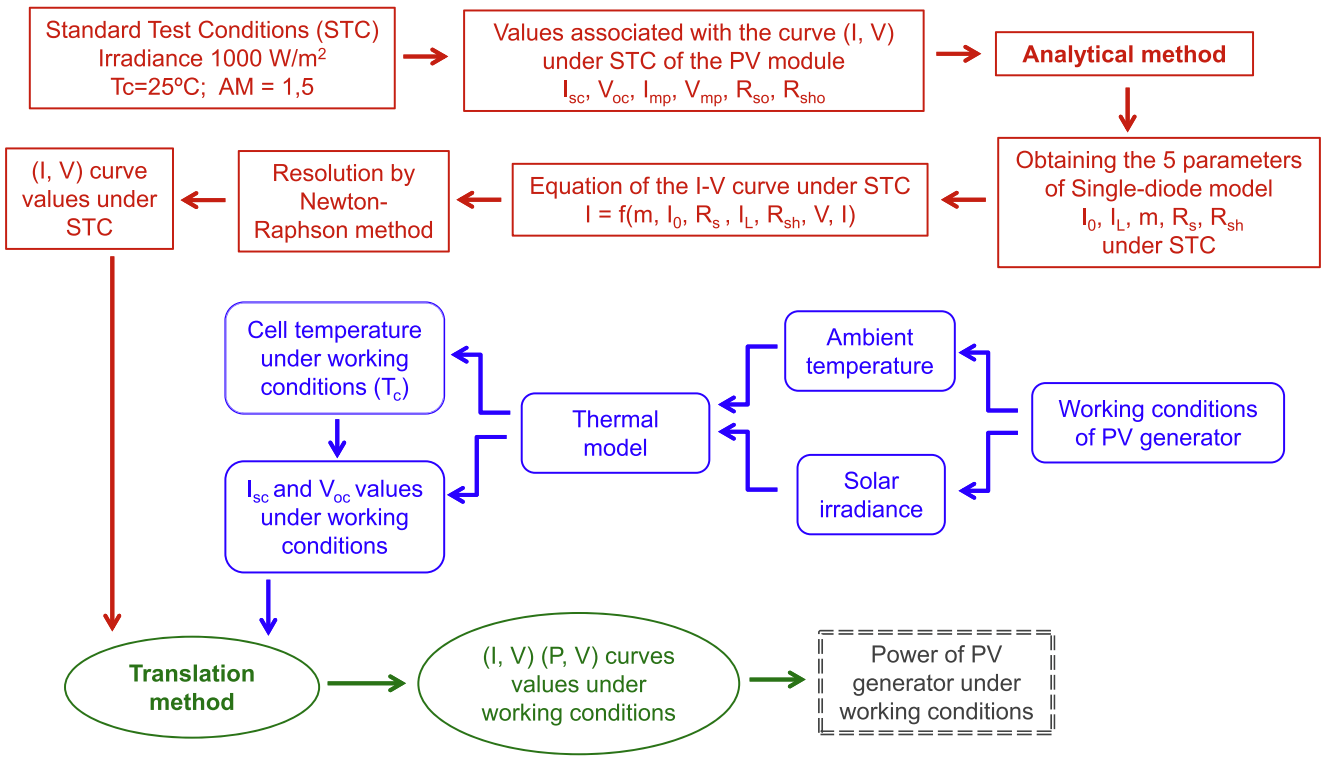

Fig. 3. Diagram of the mathematical model of the PV module and its application to determine the power generated under any working condition.

efficiency of the inverter (η_{inv}) was estimated using the model proposed by Jantsch et al. [34]:

$$\eta_{inv} = \frac{P_{out}}{P_{in}} = \frac{P_{out}}{P_{out} + powerlosses} = \frac{p_s}{p_s + c_0 + p_s c_1 + p_s^2 c_2} \quad (15)$$

where P_{in} (W) and P_{out} (W) are the input and output power from the inverter respectively, $p_s = P_{out}/P_{nom}$ (dimensionless) is the normalised output power, and P_{nom} (W) is the nominal inverter power.

The dimensionless coefficients denote different inverter power losses: c_0 represents the no-load or self-supply losses, c_1 represents the losses that depend linearly on the power (e.g. voltage drop across diodes), and c_2 represents the losses proportional to the square of the power (e.g. Joule effect).

In this work, the inverter power loss coefficients considered were $c_0 = 0.014$, $c_1 = 0.010$ and $c_2 = 0.05$, resulting in a European efficiency (η_{EUR}) of 0.926 and a maximum efficiency (η_{max}) of 0.941.

Motor-pump group

The adjusted equations q(P) obtained for each of the pumping heads tested after the experimental characterisation of the motor-pump group are summarized in Table 2 (from [23]).

The adjusted fourth-order polynomial equation q(P) obtained, allow obtaining the flow rate supplied by the pumping system at the different heads (with the distribution of the generated power between the two pumps in the desired proportion). They also allow for modelling the operation of the motor-pump group under variable power conditions. These curves were introduced into the simulation model of the PV pumping system to predict the flow rate pumped under the variable operating conditions throughout the year.

Description of the facility's simulation program

The operation of the pumping system was simulated with a program developed in LabVIEW software (LabVIEW 2018 version, National Instruments) using a personal computer. LabVIEW™ (Laboratory Virtual Instrument Engineering Workbench) is a graphical programming language, and it has powerful features for simulation.

The pumping heads considered were 18, 24, 30, 36, 42 and 48 m. The PV modules were assumed to be tilted a 35° angle and facing South. The soil albedo was taken as 0.3.

Wiring losses of 6% were assumed, including those of DC and AC. The electrical energy that feeds the motor-pump group was obtained by subtracting the losses in the wiring (in DC and AC) and the inverter from the PV energy generated. The daily/monthly/annual efficiency of the inverter was determined as the joint inverter + wiring efficiency.

The simulations were performed for Valencia (Spain) weather (39°28′13″ N, 0°22′36″ W, 21 m.a.s.l). The climatic data used were those corresponding to a TMY, a very useful tool in computer simulations for performance predictions of solar systems, such as this case [35]. In this study, the Spanish Weather for Energy Calculations (SWEC)

Table 2
Adjusted equations q(P) and regression coefficients (r^2) for the pumping group at each head (from [23]).

H (m)	REGRESSION EQUATION $q(P) = a_4 \cdot P^4 + a_3 \cdot P^3 + a_2 \cdot P^2 + a_1 \cdot P + a_0$	r^2
18	$q = -3.051 \cdot P_{mp}^4 + 10.737 \cdot P_{mp}^3 - 14.147 \cdot P_{mp}^2 + 9.146 \cdot P_{mp} - 1.2721$	0.99871
24	$q = -4.582 \cdot P_{mp}^4 + 15.942 \cdot P_{mp}^3 - 20.625 \cdot P_{mp}^2 + 12.709 \cdot P_{mp} - 2.1603$	0.99604
30	$q = -4.290 \cdot P_{mp}^4 + 16.530 \cdot P_{mp}^3 - 23.886 \cdot P_{mp}^2 + 16.236 \cdot P_{mp} - 3.4240$	0.99999
36	$q = -10.340 \cdot P_{mp}^4 + 38.341 \cdot P_{mp}^3 - 52.882 \cdot P_{mp}^2 + 33.152 \cdot P_{mp} - 7.2259$	0.99900
42	$q = -10.605 \cdot P_{mp}^4 + 40.013 \cdot P_{mp}^3 - 56.678 \cdot P_{mp}^2 + 36.835 \cdot P_{mp} - 8.6385$	0.99989
48	$q = -23.530 \cdot P_{mp}^4 + 89.984 \cdot P_{mp}^3 - 128.820 \cdot P_{mp}^2 + 83.039 \cdot P_{mp} - 19.865$	0.99999
54	$q = 23.563 \cdot P_{mp}^4 - 60.966 \cdot P_{mp}^3 + 45.190 \cdot P_{mp}^2 - 0.386 \cdot P_{mp} - 6.746$	0.99980

database [36], developed by the Grupo de Termotecnia of the Escuela Superior de Ingenieros in Seville for the Spanish Government, was employed. The generated TMY included hourly data of horizontal global solar irradiance and ambient temperature for 365 days a year.

The combination of the mathematical model of the PV generator, with the equations that relate the VSD input and output electrical power, the equations that relate the electrical power supplied to the motor-pump group, and the flow rate supplied as a function of pumping head, structure the simulation model of the PV pumping facility.

The process of calculating the flow rate pumped by the motor-pump group depending on the working conditions, requires the definition of several task blocks. These blocks are the following: definition of pumping conditions and working conditions; calculation of the solar irradiance on the plane of the PV generator from the solar irradiance on the horizontal plane; calculation of the (I-V) curve of the PV generator in STC and extraction of its characteristic parameters; calculation of the (I-V) curve in working conditions and calculation of the generated power; estimation of inverter efficiency and losses in wiring as well as other energy losses; calculation of the power supplied to the motor-pump group and the pumped flow.

This calculation process is repeated for each time interval into which the simulation period is divided (in the case study every hour throughout a full year).

The LabVIEW PV system simulation program is described below. It integrates the different calculation subprograms for the different simulation stages and the single control program that executes the sequential calculation throughput the simulated year.

Calculation subprogrammes

The following stages are executed:

- Definition of pumping conditions and working conditions.
- Obtaining the solar irradiance on a tilted surface. The Hay, Klucher and Reindl (HDKR) anisotropic correlation model [37] was used to obtain the values of solar irradiance on the plane of the PV generator (W/m^2).

In this subprogram, the input data were global hourly solar irradiance on horizontal surface (W/m^2), daytime hours, Julian day of the year, tilt (degrees), latitude, and albedo. The output results were solar declination and solar hour angles (degrees), extraterrestrial solar irradiance on horizontal surface (W/m^2), direct and diffuse solar irradiance on tilted surface and on horizontal surface (W/m^2), atmospheric transparency index, and global hourly solar irradiance on tilted surface (W/m^2).

- Consideration of losses of the incident solar radiation due to angular effects and dust on the modules.
- Application of the single-diode PV cell model and obtaining the 5 parameters of the analytical equation corresponding to the curve (I-V) of the PV module in STC.

In this subprogram, the input data were the data provided in the manufacturer's catalogue (values of V_{oc}, I_{sc}, V_{mp}, I_{mp}, TONC, α_I, and β_V in Table 1), in addition to R_{so} and R_{sho} (estimated from the slopes of the I-V curve at SC and OC respectively), peak power (Wp), and cell temperature T_c (K). The output results were the five parameters of the single-diode model (I_0, I_L, m, R_s, and R_{sh}), and the (I-V) and (P-V) curves in STC.

- Application of the translation method and the thermal model to obtain the points of the characteristic curve (I-V) at working conditions. Obtaining the maximum power point of the PV module under these conditions and the electrical power produced by the PV generator.

In this subprogram, the input data were global solar irradiance on the tilted surface (W/m^2) corresponding to the working conditions of the time of day in which the calculation is performed, hourly ambient temperature in °C (corresponding to the same time of day), PV generator working voltage (V), and configuration of the PV generator with the number of modules connected in series and in parallel. The output results were the (I-V) and (V-P) curves in working conditions, the values associated with the curve (I-V) of the PV module: I_{sc}, V_{oc}, I_{mp}, V_{mp}, R_{so}, R_{sho}, P_{max}, as well as the voltage, current and power supplied by the PV generator in the same working conditions.

- Consideration of the inverter's efficiency and wiring losses. Determination of the electrical power applied to the motor-pumps.

Control program. Simulation of the PV pumping system

This program controls the implementation of the previous subprogrammes and also performs the necessary calculations to determine the pumped flow rate in each hourly period.

With this purpose, the pumped flow rate was calculated from the electrical power supplied to the two motor-pump groups and the head at which it is desired to pump by applying the equations q(P) for each head (Table 2).

The electric power is either distributed between the two motor-pump groups at 50% or the strategy of power division proposed is applied.

The control program also performs a temporary integration of the results to determine the available energy and the volume of water pumped each day of the year. Finally, it organises the hourly and daily results and sends them to a data storage file for later processing in a spreadsheet. From the power supplied by the VSD to the motor-pump group and the pumping head, the pumped flow rate can be determined.

Fig. 4 shows the work sequence of the simulation program.

Study and comparative analysis

The facility's performance at all the considered pumping heads was simulated under the two different working conditions referred to as Distribution at 50% and Strategy. The alternatives depicted in Fig. 5 consisted of:

Distribution at 50%

The PV power generated is always distributed at 50% between the two pumps regardless of the available power. This option is equivalent to assuming the facility is equipped with two equal PV generators (an individual PV generator for each pump). Each generator transfers the electrical power generated to its corresponding FC/motor-pump group.

Strategy

The division of the generated power between the two pumps is accomplished by applying the method for distributing the power generated in a pumping system with two equal pumps and a single PV generator investigated in [23]. The PV power coming from the generator is transferred to each pump via the corresponding FC, which can modulate the power supplied via the frequency/output voltage control.

The simulations were carried out over a full year. The comparison of the two working conditions was made from the determination, in each case, of both the pumped volume and the efficiency of the pumping group at the different pumping heads.

Results and discussion

Incident solar radiation and generated electric energy

Fig. 6 shows the monthly values throughout a year of both the incident solar irradiation (SI) on the horizontal plane (generated from the TMY) and the SI on the plane of PV generator (obtained from the HDKR anisotropic correlation model). The effective SI on a tilted surface

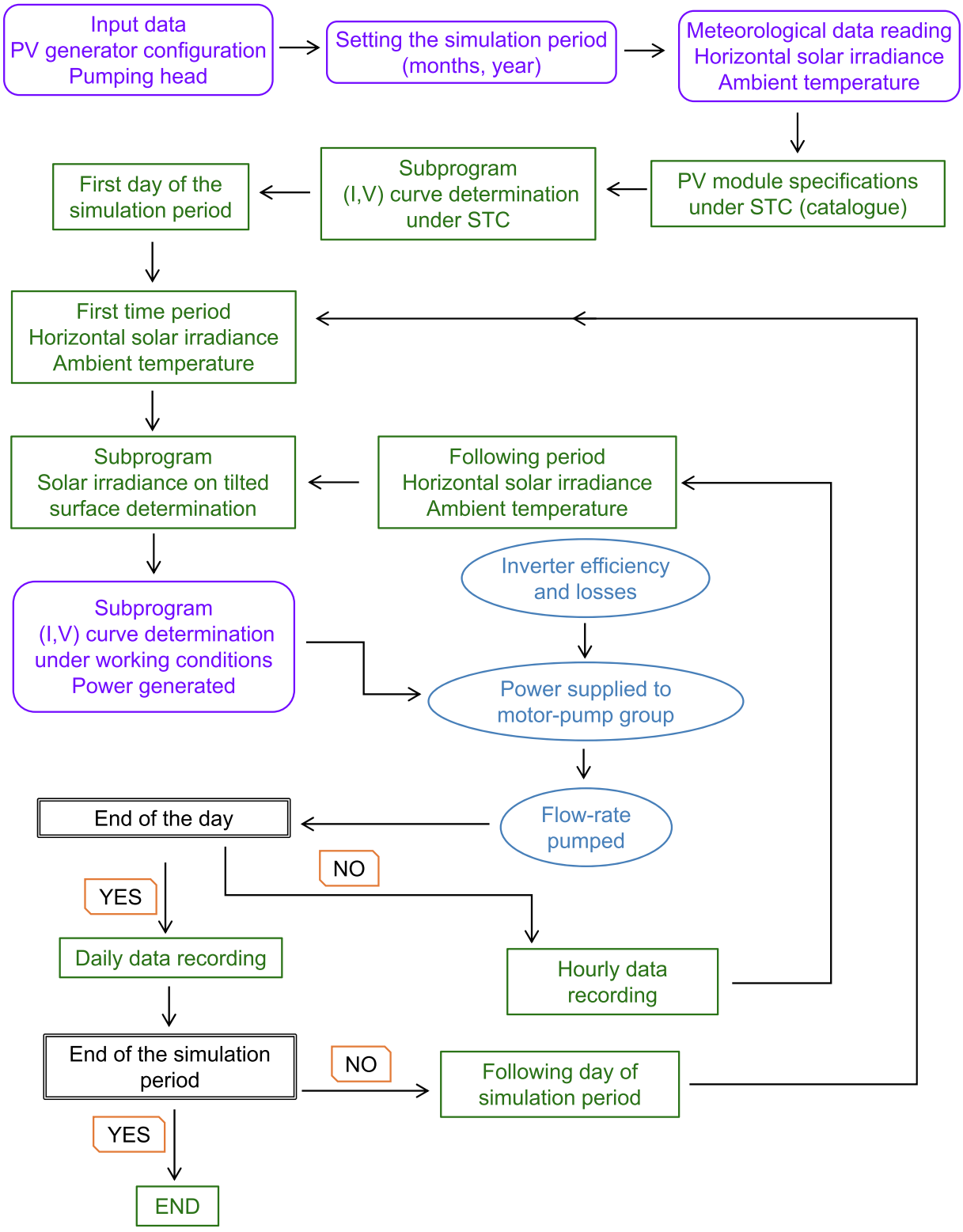

Fig. 4. Work sequence of the simulation program of the PV pumping system.

after considering reflection and dirt losses on the surface of PV modules is also included.

The results derived from applying the mathematical model of the PV module to determine the monthly values of the electric energy generated and the power supplied to the motor-pump group are shown in Fig. 7.

The corresponding annual values of the incident SI and the electrical energy generated by the PV facility can be seen in Table 3.

Simulation of the PV system

Volume pumped and efficiency of the motor-pump group with each of the two alternatives for the distribution of generated power between the two pumps

Fig. 8 shows the results of the PV system simulation concerning the total annual volume pumped (m^3) at the different heads and considering

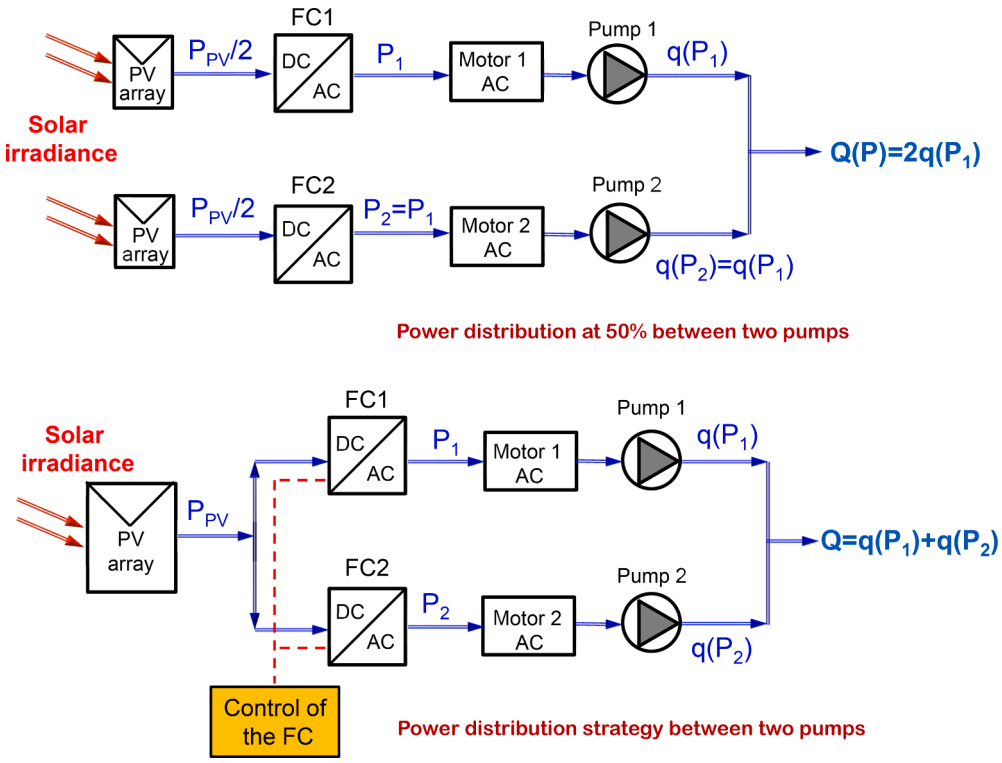

Fig. 5. Alternatives of power distribution compared in this study.

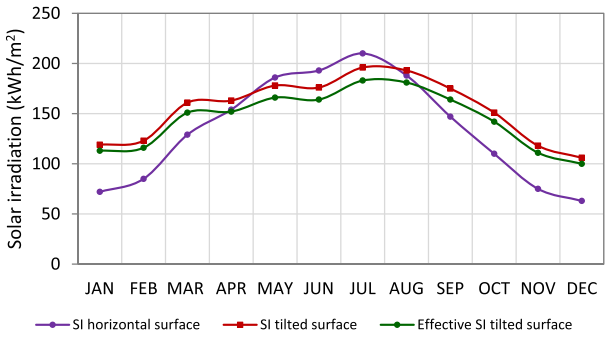

Fig. 6. Monthly values of incident solar irradiation (SI) on the horizontal surface (TMY), SI on the tilted surface of the PV modules (HDKR model), and the effective value of the latter considering the losses by reflection and dirt on the PV modules.

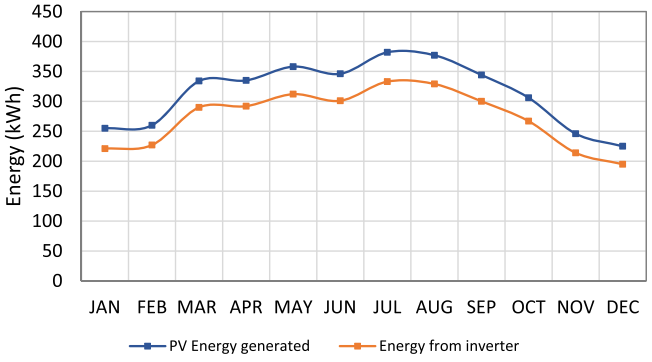

Fig. 7. Results of the simulation for the monthly energy provided by the PV generator and the energy that supplies the motor-pump group.

Table 3
Annual values of incident SI and electrical energy generated by the PV facility.

	Annual value
Horizontal SI (kWh/m^2)	1612
SI on tilted surface 35° South (kWh/m^2)	1859
PV Energy generated (kWh)	4006
Electric energy to the motor-pump group (kWh)	3587

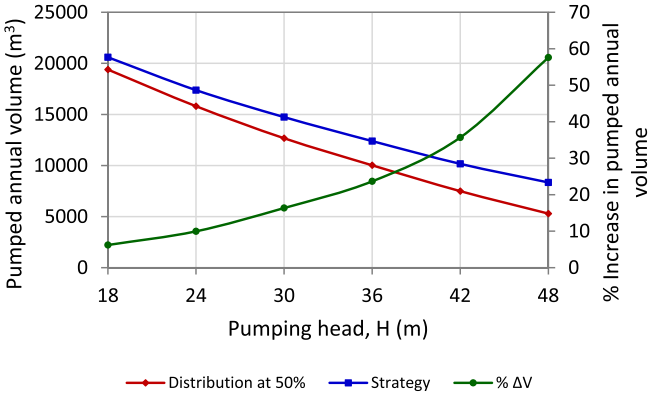

Fig. 8. Total pumped annual volume (m^3) considering the two operating alternatives. Increase in pumped annual volume (%) when applying the power distribution strategy.

the two simulated alternatives, Distribution at 50%, and Strategy. The increase in pumped annual volume (expressed as %) obtained with the Strategy compared to that obtained with the Distribution at 50% is also represented.

An increase in pumped annual volume is observed at all heads when the Strategy is applied.

The pumped annual volume logically decreases with head in both

cases. Nevertheless, this decrease is more pronounced with the Distribution at 50% and the higher the head, the greater the difference between the two situations analysed. Consequently, the increase in pumped annual volume when the Strategy is applied compared to the Distribution at 50% also growths progressively with head, going from 6.21% (H = 18 m) to 57.60% (H = 48 m).

Fig. 9 shows the results of the annual efficiency of the motor-pump group at the different heads with the two simulated operating modes. The increase in annual efficiency applying the Strategy compared to that achieved with the Distribution at 50%, expressed as a percentage, is also depicted.

As can be seen, when the pumping system operates with Strategy, the motor-pump group works with greater efficiency for all heads and the higher the head, the greater the difference in annual efficiency between the two alternatives. The increase in annual efficiency applying the Strategy compared to Distribution at 50% goes from 6.42% for H = 18 m to 57.51% for H = 48 m. Adopting the Strategy also allows maintaining high efficiency of the motor-pump group at all the heads. In the case of Distribution at 50%, the efficiency decreases strongly at the highest heads (42 and 48 m).

When considering the monthly efficiency of the motor-pump group throughout the year (Fig. 10), the same pattern is observed. The efficiency of the motor-pump group when establishing the Strategy is higher at all pumping heads, as well as considerably more uniform throughout the months of the year than when Distribution at 50% is applied.

Analysis of daily results

To check what causes the improvement in annual and monthly outcomes, a detailed analysis comparing the two operating alternatives during a day was performed. As the annual increase in pumped volume with Strategy compared to Distribution at 50% in the case H = 36 m (23.7%, Fig. 9) and the increase in pumped volume in July (21.6%) are similar in order of magnitude, and since on July 29 a comparable increase in pumped volume (23.3%) was also obtained, the day July 29 and pumping at H = 36 m were selected for this analysis.

Fig. 11 shows the results obtained on July 29 for the daily evolution of the incident solar irradiance on the plane of the PV generator and the flow rates (L/s) pumped with the two alternatives for the distribution of the generated power. During the early afternoon, coinciding with the hours of higher solar irradiance, the flow rate pumped with both operating options is similar. However, when the pumping strategy is adopted, pumping starts earlier and ends later, indicating lower pumping threshold irradiance.

Fig. 12 shows the results obtained on July 29 and H = 36 m relative to the electrical power that feeds the pumping group throughout the day and the efficiency of the motor-pump group for the two power distribution cases. With the pumping strategy, less electrical power is needed to start pumping and, at certain hours at the beginning and end of the day, the efficiency of the motor-pump group is greater.

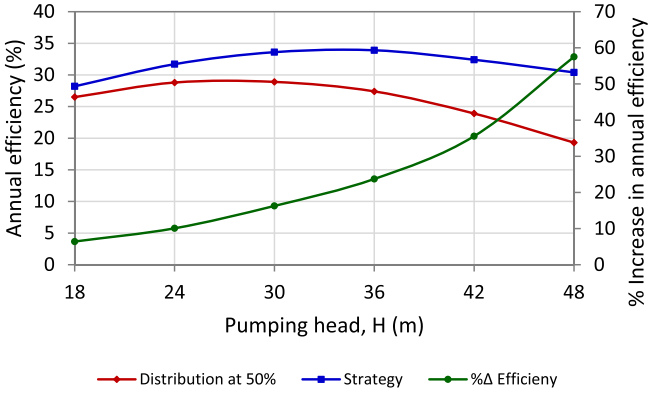

Fig. 9. Annual efficiency of the motor-pump group with the two operating modes. Annual efficiency increase (%) when the Strategy is applied.

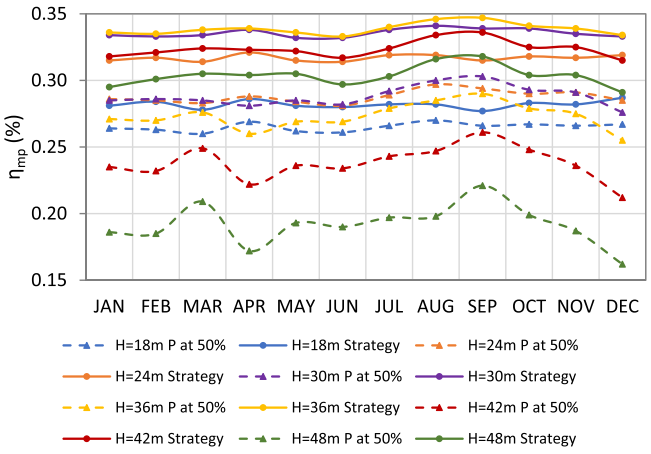

Fig. 10. Monthly efficiency of the motor-pump group throughout the year with Strategy (solid lines) and with Distribution at 50% (dashed lines).

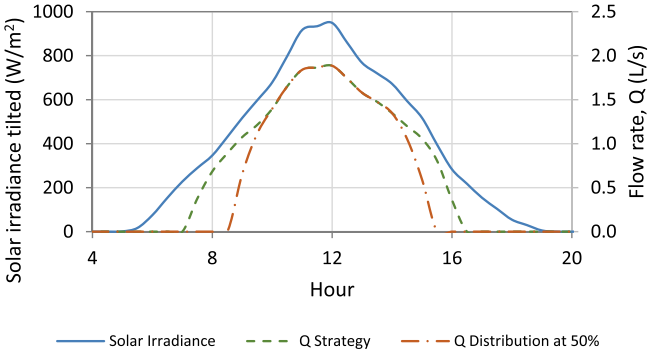

Fig. 11. Daily evolution (July 29, H = 36 m) of the incident solar irradiance (W/m^2) on the plane of the PV generator, and of the pumped flow rates (L/s) with the two distribution alternatives of the generated power.

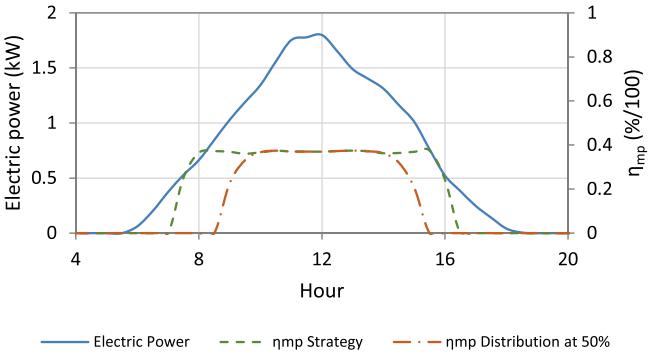

Fig. 12. Daily evolution (July 29, H = 36 m) of the electrical power (kW) that feeds the pumping group, and of the efficiency of the motor-pump group (%/100) with the two alternatives for the distribution of the generated power.

The daily results that summarize the difference in pumping behaviour are shown in Table 4. The two circumstances that explain the increase in daily pumped volume, which goes from 32.75 to 40.39 m^3/day (representing an increase of 23.3%), when the Strategy is applied are:

1) The reduction of the pumping threshold irradiance, which is 517.2 W/m^2 with Distribution at 50%, versus 289.4 W/m^2 with Strategy. Pumping starts before and ends later operating with the pumping

Table 4
Reference parameters for the comparative analysis of the two pumping alternatives relative to July 29 and H = 36 m. Pumped volume (m^3), pumping threshold irradiance (W/m^2) and efficiency of the motor-pump group.

July 29H = 36 m	Pumped volume m^3/day	Irradiance threshold for pumping (W/m^2)	Efficiency motor-pump (%)
Distribution at 50%	32.75	517.2	34.8
Strategy	40.39	289.4	36.4

strategy, and therefore, lower levels of solar irradiance are required for pumping at the beginning and end of the day.

2) The pumping group works with better efficiency during the pumping period: 36.4% (Strategy) vs. 34.8% (Distribution at 50%).

When studying the efficiency of the motor-pump group as a function of electrical energy with both alternatives at H = 36 m (Fig. 13), it is verified that pumping with Strategy starts with half the energy supplied by the PV generator (0.44 kW with Strategy vs. 0.88 kW with Distribution at 50%). This is justified because, in the latter case, the power is divided between the two pumps, which start operating simultaneously. This explains the lower pumping threshold irradiance observed with the Strategy.

Once the power required to start pumping in the case of operation with Distribution at 50% is reached, there is a range of powers (from 0.88 to 1.24 kW) in which a single group is operating in the case of Strategy with higher efficiency throughout all the range, while in the case of Distribution at 50%, both groups are pumping with much lower efficiency. This situation continues until the second pump is connected in the Strategy case, for power supplies greater than 1.24 kW. From this point onwards, the pumping group efficiency and therefore the pumped flow rate with both operating options, are identical, as indicated in Fig. 13. This situation normally takes place during the hours of greatest solar irradiance. When the irradiance level decreases towards the end of the day, the opposite happens.

It should be noted that the same pattern is observed every day of the year and at any other pumping head.

Finally, it is also worth mentioning that the same study was conducted in a PV facility with two 1.5 kW pumping groups working in parallel and the same conclusions (not reported here) were drawn. This confirms the applicability of the proposed pumping strategy to pumps of higher powers.

Conclusions

The suitability of the strategy for distributing the power coming from a PV generator between two equal pumps working in parallel proposed in [23] was verified. This strategy consists of feeding a single pump with all the power generated until it exceeds a threshold value from which the power distribution must be at 50% between the two pumps.

Pumping by applying the strategy was compared to pumping with the generated power distribution at 50% between the two motor-pump groups regardless the available power. For this purpose, a system equipped with two pumping groups, 0.75 kW each, was employed. The assessment of the facility's performance under both alternative working conditions and at several pumping heads was conducted using simulation techniques. The pumped flow rate, the total pumped volume, and the efficiency of the facility in each case were determined in an hourly, daily and monthly basis for a whole year.

For all heads, the operation with power distribution according to the proposed Strategy increased the pumped annual volume compared to Distribution at 50%. This difference increased progressively with head, in accordance with the improvement in annual efficiency. Moreover, the efficiency of the motor-pump group when establishing the Strategy was higher at each pumping head as well as considerably more uniform throughout the months of the year than with the Distribution at 50%.

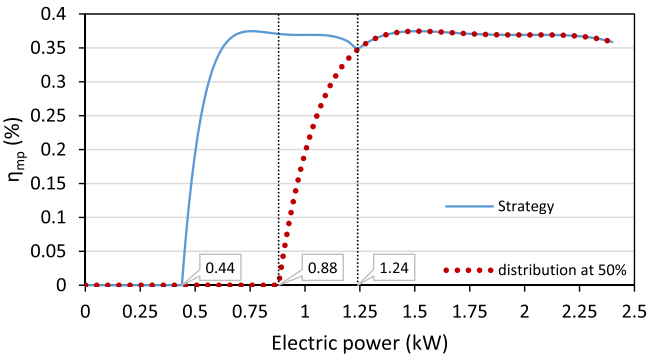

Fig. 13. Efficiencies of the motor-pump groups as a function of the electrical power supplied, with the two distribution alternatives for the power generated. Results obtained on July 29 and H = 36 m.

The detailed daily analysis showed an increase of 23.3% in daily pumped volume, when the Strategy is applied. Two circumstances explain this increase, the halving of the solar irradiance threshold and the efficiency improvement during the pumping period: 36.4% (Strategy) compared to 34.8% (Distribution at 50%).

When studying the efficiency of the motor-pump groups as a function of electrical energy with both pumping alternatives during a day, it was verified that pumping with Strategy starts with half the energy supplied by the PV generator. Once the power required to start pumping in the case of operation with Distribution at 50% is reached, there is a range of powers in which a single group is pumping, in the case of Strategy, with greater efficiency, while in the case of Distribution at 50% both groups are working with much lower efficiency. This situation continues until the hours of greatest solar irradiance arrive, when the second pump is connected in the Strategy case. From this point onwards, the efficiency and therefore the pumped flow rate with both operating options are similar. When the irradiance level decreases towards the end of the day, the opposite happens.

The proposal for dividing the generated power investigated and applied in this study optimises the energy management in a PV pumping system with two equal parallel pumps compared with the operating mode usually applied in these facilities with the distribution of the generated power at 50% between the two pumps (equivalent to feeding each pump with a single PV generator half the size).

Similar results were drawn in a PV facility equipped with two pumping groups 1.5 kW each (results not reported in this paper). This confirms that the conclusions derived from this work can be extrapolated to pumps of higher powers.

Further work is in progress related to the study of pumping groups with higher numbers of pumps in parallel. The application of the strategy for distributing the generated power with higher numbers of pumps would allow to improve the facility's performance.

CRediT authorship contribution statement

María Gasque: Data curation, Formal analysis, Writing - original draft, Writing - review & editing. **Pablo González-Altozano:** Data curation, Formal analysis, Writing - original draft. **Rosa Penélope Gutiérrez-Colomer:** Data curation, Formal analysis. **Eugenio García-Marí:** Conceptualization, Data curation, Formal analysis, Writing - original draft.

Declaration of Competing Interest

The authors declare that they have no known competing financial interests or personal relationships that could have appeared to influence

the work reported in this paper.

References

[1] Lacal-Arántegui R, Jäger-Waldau A. Photovoltaics and wind status in the European Union after the Paris Agreement. Renew Sustain Energy Rev 2018;81:2460–71. https://doi.org/10.1016/j.rser.2017.06.052.

[2] Gielen D, Boshell F, Saygin D, Bazilian MD, Wagner N, Gorin R. The role of renewable energy in the global energy transformation. Energy Strateg Rev 2019; 24:38–50. https://doi.org/10.1016/j.esr.2019.01.006.

[3] Shivakumar A, Dobbins A, Fahl U, Singh A. Drivers of renewable energy deployment in the EU: an analysis of past trends and projections. Energy Strategy Rev 2019;26:100402-. https://doi.org/10.1016/j.esr.2019.100402.

[4] FAO. Hartung H, Pluschke L. The benefits and risks of solar-powered irrigation – a global review; 2018.

[5] Ramos JS, Ramos HM. Solar powered pumps to supply water for rural or isolated zones: a case study. Energy Sustain Dev 2009;13:151–8. https://doi.org/10.1016/j.esd.2009.06.006.

[6] Allouhi A, Buker MS, El-houari H, Boharb A, Benzakour Amine M, Kousksou T, et al. PV water pumping systems for domestic uses in remote areas: sizing process, simulation and economic evaluation. Renew Energy 2019;132:798–812. https://doi.org/10.1016/j.renene.2018.08.019.

[7] Chandel SS, Naik MN, Chandel R. Review of solar photovoltaic water pumping system technology for irrigation and community drinking water supplies. Renew Sust Energy Rev 2015;49:1084–99. https://doi.org/10.1016/j.rser.2015.04.083.

[8] Wazed SM, Hughes BR, O'Connor D, Calautit K. A review of sustainable solar irrigation systems for Sub-Saharan Africa. Renew Sust Energy Rev 2018;81: 1206–25. https://doi.org/10.1016/j.rser.2017.08.039.

[9] Jadhav PJ, Sawant N, Panicker AM. Technical paradigms in electricity supply for irrigation pumps: case of Maharashtra, India. Energy Sustain Dev 2020;58:50–62. https://doi.org/10.1016/j.esd.2020.07.005.

[10] López-Luque R, Reca J, Martínez J. Optimal design of a standalone direct pumping photovoltaic system for deficit irrigation of olive orchards. Appl Energy 2015;149: 13–23. https://doi.org/10.1016/j.apenergy.2015.03.107.

[11] García-Tejero IF, Durán-Zuazo VH, editors. Water scarcity and sustainable agriculture in semiarid environment. Tools, strategies and challenges for woody crops. 1st ed. Academic Press; 2018.

[12] Todde G, Murgia L, Deligios PA, Hogan R, Carrelo I, Moreira M, et al. Energy and environmental performances of hybrid photovoltaic irrigation systems in Mediterranean intensive and super-intensive olive orchards. Sci Total Environ 2019;651:2514–23. https://doi.org/10.1016/j.scitotenv.2018.10.175.

[13] Aliyu M, Hassan G, Said SA, Siddiqui MU, Alawami AT, Elamin IM. A review of solar powered water pumping systems. Renew Sust Energy Rev 2018;87:61–76. https://doi.org/10.1016/j.rser.2018.02.010.

[14] Rekioua D, Matange E. Optimization of photovoltaic power systems. Modelization, simulation and control. London: Springer Verlag; 2012.

[15] Shepovalov OV, Belenov AT, Chirkov SV. Review of photovoltaic water pumping system research. Energy Rep 2020;6:306–24. https://doi.org/10.1016/j.egyr.2020.08.053.

[16] Almeida RH, Ledesma JR, Carrêlo IB, Narvarte L, Ferrara G, Antipodi L. A new pump selection method for large-power PV irrigation systems at a variable frequency. Energy Convers Manage 2018;174:874–85. https://doi.org/10.1016/j.enconman.2018.08.071.

[17] Matam M, Barry VR, Govind AR. Optimized Reconfigurable PV array-based Photovoltaic water-pumping system. Sol Energy 2018;170:1063–73. https://doi.org/10.1016/j.solener.2018.05.046.

[18] Narvarte L, Fernández-Ramos J, Martínez-Moreno F, Carrasco LM, Almeida RH, Carrêlo IB. Solutions for adapting photovoltaics to large power irrigation systems for agriculture. Sustain Energy Technol Assess 2018;29:119–30. https://doi.org/10.1016/j.seta.2018.07.004.

[19] Talbi B, Krim F, Rekioua T, Mekhilef S, Laib A, Belaout A. A high-performance control scheme for photovoltaic pumping system under sudden irradiance and load changes. Sol Energy 2018;159:353–68. https://doi.org/10.1016/j.solener.2017.11.009.

[20] Poompavai T, Kowsalya M. Control and energy management strategies applied for solar photovoltaic and wind energy fed water pumping system: a review. Renew Sust Energy Rev 2019;107:108–22. https://doi.org/10.1016/j.rser.2019.02.023.

[21] Zavala V, López-Luque R, Reca J, Martínez J, Lao MT. Optimal management of a multisector standalone direct pumping photovoltaic irrigation system. Appl Energy 2020;260:114261. https://doi.org/10.1016/j.apenergy.2019.114261.

[22] Harkani A, Oudadda M, El Fihri FH, El Aissaoui A. Performance management of photovoltaic parallel pumps for optimal hydraulic power point tracking. Int J Renew Energy Res 2019;9(3):1398–405.

[23] Gasque M, González-Altozano P, Gutiérrez-Colomer RP, García-Marí E. Optimisation of the distribution of power from a photovoltaic generator between two pumps working in parallel. Sol Energy 2020;198:324–34. https://doi.org/10.1016/j.solener.2020.01.013.

[24] Atersa manufacturer datasheet. http://www.solytek.es/pdfs/-var-www-html-typo3Live-fileadmin-atersa-catalogos-ES-1-Modulos.pdf [accessed 07 December 2020].

[25] Franklin Electric Europa GmbH. 4" Encapsulated Motors. Product Information and Service. https://franklinwater.eu/products/submersible-motors/franklin-electric/4-encapsulated-motors/; 2015 [accessed 07 December 2020].

[26] Phang JCH, Chan DSH, Philips JR. Accurate analytical method for the extraction of solar cell model parameters. Electron Let 1984;20(10):406–8.

[27] de Blas MA, Torres JL, Prieto E, García A. Selecting a suitable model for characterizing photovoltaic devices. Renew Energy 2002;25(3):371–80. https://doi.org/10.1016/S0960-1481(01)00056-8.

[28] Celik AN, Acikgoz N. Modelling and experimental verification of the operating current of monocrystalline photovoltaic modules using four-and five-parameter models. Appl Energy 2007;84:1–15. https://doi.org/10.1016/j.apenergy.2006.04.007.

[29] Ibrahim H, Anani N. Evaluation of analytical methods for parameter extraction of PV modules. Energy Procedia 2017;134:69–78. https://doi.org/10.1016/j.egypro.2017.09.601.

[30] Hadj Arab A, Chenlo F, Benghanem M. Loss-of-load probability of photovoltaic water pumping systems. Sol Energy 2004;76:713–23. https://doi.org/10.1016/j.solener.2004.01.006.

[31] Drouiche I, Harrouni S, Hadj AA. A new approach for modelling the aging PV module upon experimental I-V curves by combining translation method and five-parameters model. Electr Pow Syst Res 2018;163:231–41. https://doi.org/10.1016/j.epsr.2018.06.014.

[32] Martin N, Ruiz JM. Calculation of the PV modules angular losses under field conditions by means of an analytical model. Solar Energ Mater Solar Cells 2001; 70: 25-38. doi:10.1016/S0927-0248(00)00408-6.

[33] Reca J, López-Luque R. Chapter 9—Design Principles of Photovoltaic Irrigation Systems. In: Yahyaoui I, editor. Advances in Renewable Energies and Power Technologies. Elsevier Science: Amsterdam, The Netherlands; 2018, p. 295–333. doi:10.1016/B978-0-12-812959-3.00009-5.

[34] Jantsch M, Schmidt H, Schmid J. Results on the concerted action on power conditioning and control. In 11th European Photovoltaic Solar Energy Conference, Montreux, Switzerland; 1992, p.1589-92.

[35] Kalogirou SA. Generation of Typical Meteorological Year (TMY-2) for Nicosia, Cyprus. Renew Energy 2003;28(15):2317–34. https://doi.org/10.1016/S0960-1481(03)00131-9.

[36] SWEC (Spanish Weather for Energy Calculations) https://energyplus.net/weather-region/europe_wmo_region_6/ESP%20%20 [accessed 07 December 2020].

[37] Duffie JA, Beckman WA. Solar engineering of thermal process. 4th ed. Wiley: John Wiley & Sons; 2013.